Computational Studies of the Electronic Structures of Copper-Doped CdSe Nanocrystals: Oxidation States, Jahn−Teller Distortions, Vibronic Bandshapes, and Singlet−Triplet Splittings

Heidi D. Nelson, Xiaosong Li, and Daniel R. Gamelin*

Department of Chemistry, University of Washington, Seattle, WA 98195-1700, United States
Email: gamelin@chem.washington.edu

Table S1. Calculated forces and displacements for the ground-state geometry optimization of the Cu^+:$Cd_{33}Se_{34}$ structure, using the default threshold set by Gaussian and a higher threshold (keyword opt=tight).

	Default threshold			Higher threshold (opt=tight)		
	Threshold	Value (est. 2nd deriv.)	Value (calc. 2nd deriv.)	Threshold	Value (est. 2nd deriv.)	Value (calc. 2nd deriv.)
Max. force	0.000450	0.000073	0.000212	0.000015	0.000009	0.000212
RMS force	0.000300	0.000008	0.000033	0.000010	0.000001	0.000035
Max. displacement	0.001800	0.001453	0.049797	0.000060	0.000021	0.049841
RMS displacement	0.001200	0.000165	0.006584	0.000040	0.000003	0.006552

The optimization calculation uses estimated second derivatives and indicates that the structure has converged, but calculating the second derivative indicates that a true stationary point has not been reached. Changing the thresholds used in the optimization calculation appears to improve the obtained values, but the geometry does not change significantly and the second derivative calculation shows that a stationary point still has not been reached. Because changing the optimization thresholds does not significantly change the resulting energy or geometry, and because the forces are small in all cases, we conclude that the potential energy surface is very flat in this region and the calculated energy and geometry are very close to the true minimum. These results could potentially be improved by calculating the second derivatives at every step of the optimization (using keyword opt=CalcFC in Gaussian), but this approach is too computationally expensive to be practical, especially for the larger NC structures and the excited-state optimization calculations. Therefore, the results reported here are for structures that are converged according to the default threshold with estimated second derivatives.
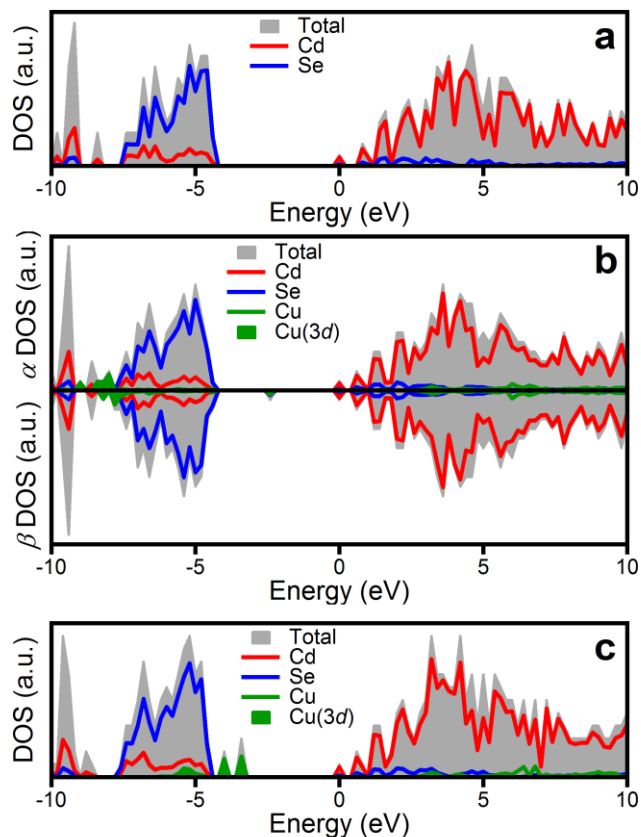
Figure S1. Calculated densities of states (DOS) for **(a)** $Cd_{34}Se_{34}$, **(b)** $Cu^{2+}:Cd_{33}Se_{34}$, and **(c)** $Cu^{+}:Cd_{33}Se_{34}$ NCs. The total DOS is shown in solid gray, while the partial DOS is shown as red lines for Cd ($4d$, $5s$, $5p$), blue lines for Se ($4s$, $4p$), and green lines for Cu ($3d$, $4s$, $4p$). The Cu($3d$) character in the doped NCs is further highlighted in solid green. For the Cu^{2+}-doped NC, which has an open-shell configuration, the α and β DOS are represented by positive and negative values, respectively. These densities of states provide an alternative representation of the molecular-orbital energies shown in Figure 1 of the main text.

Table S2. Calculated atomic orbital contributions (as percentages) to selected copper-based molecular orbitals in Cu^{2+}:$Cd_{33}Se_{34}$, Cu^{+}:$Cd_{33}Se_{34}$, and Cu^{+}:$Cd_{76}Se_{77}$ NCs.

Atomic orbital	Cu^{2+}:$Cd_{33}Se_{34}$ LUMO	Cu^{+}:$Cd_{33}Se_{34}$ HOMO	Cu^{+}:$Cd_{76}Se_{77}$ HOMO
Cu(3d)	38.4	50.2	45.6
Cu(4s)	0.0	0.0	0.0
Cu(4p)	3.4	2.7	2.8
Cd(4d)	0.9	0.9	1.0
Cd(5s)	2.9	2.1	2.1
Cd(5p)	4.3	4.2	4.3
Se(4s)	1.1	0.9	0.9
Se(4p)	47.6	38.4	42.8
H(1s)	1.6	0.8	0.4
Total Cu	41.8	52.8	48.4
Total Cd	8.1	7.2	7.5
Total Se	48.6	39.2	43.7

All of these molecular orbitals have primarily Cu(3d) and Se(4p) character. The LUMO of the Cu^{2+}-doped NC is similar to the HOMO of the Cu^{+}-doped NC (as shown in Figure 1 and discussed in the main text). The Se(4p) contribution to the HOMO of the Cu^{+}-doped NCs increases with increasing NC size, consistent with the trend in binding energy discussed in the main text.
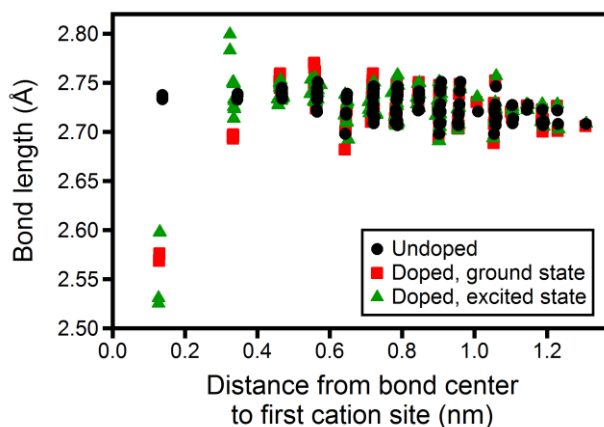

Figure S2. Calculated bond lengths for all Cu−Se and Cd−Se bonds in the ground state of an undoped $Cd_{77}Se_{77}$ NC (black circles) and the ground state (red squares) and the lowest-energy $^{1}ML_{CB}CT$ excited state (green triangles) of a Cu^{+}:$Cd_{76}Se_{77}$ NC. In the undoped NC and the ground state of the Cu^{+}-doped NC, the symmetry around the first cation site (the site occupied by the Cu^{+} dopant) is very close to tetrahedral, while the symmetry is clearly broken in the excited state due to the Jahn−Teller distortion. Replacing Cd^{2+} with Cu^{+} causes a large contraction of the lattice around the dopant; these bond length changes are larger than the bond length changes between the ground state and the excited state. The distortion associated with Cu^{+} doping and the distortion associated with the $ML_{CB}CT$ excited state are both centered around the dopant and cause minimal changes in Cd−Se bond lengths elsewhere in the lattice.
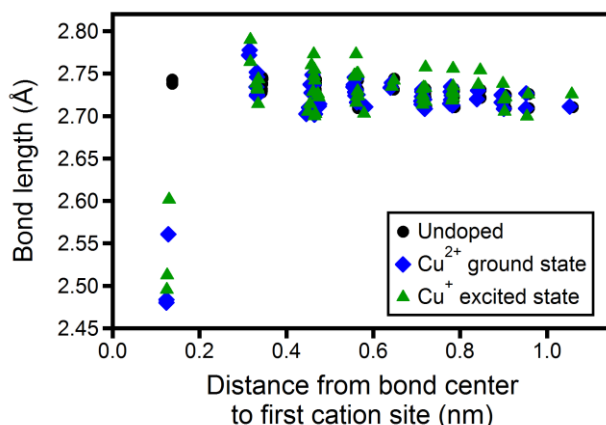
Figure S3. Calculated bond lengths for all Cu−Se and Cd−Se bonds in the ground state of a undoped $Cd_{34}Se_{34}$ NC (black circles), the ground state of a Cu^{2+}:$Cd_{33}Se_{34}$ NC (blue diamonds), and the lowest-energy $^1ML_{CB}CT$ excited state of a Cu^+:$Cd_{33}Se_{34}$ NC (green triangles). In both the ground state of the Cu^{2+}-doped NC (Table S3) and the excited state of the Cu^+-doped NC (Table S4), the Cu^{2+} character of the dopant results in a net contraction and asymmetric Jahn−Teller distortion around the dopant site. The other Cd−Se bond lengths in these distorted states are also similar.

Table S3. Calculated ground-state geometry (Cd−Se or Cu−Se bond lengths, Se−Cd−Se or Se−Cu−Se bond angles, and dihedral angles) around the first cation site (the site occupied by the Cu dopant in the doped NCs) for $Cd_{34}Se_{34}$, Cu^{2+}:$Cd_{33}Se_{34}$, and Cu^+:$Cd_{33}Se_{34}$ NCs. Atom 1 is the cation (Cd^{2+}, Cu^{2+}, or Cu^+) and atoms 2−5 are the adjacent Se^{2-} anions.

	Undoped	Cu^{2+}-doped	Cu^+-doped
r_{12} (Å)	2.738	2.561	2.579
r_{13} (Å)	2.738	2.561	2.579
r_{14} (Å)	2.743	2.480	2.580
r_{15} (Å)	2.742	2.484	2.579
θ_{213}	109.8	111.2	109.8
θ_{214}	109.4	110.9	109.3
θ_{215}	109.6	112.0	109.7
θ_{314}	109.4	110.9	109.3
θ_{315}	109.6	112.0	109.7
θ_{415}	109.6	99.3	109.1
D_{5423}	70.6	72.8	70.6
D_{5234}	70.4	63.5	70.4
D_{5342}	70.6	72.8	70.6

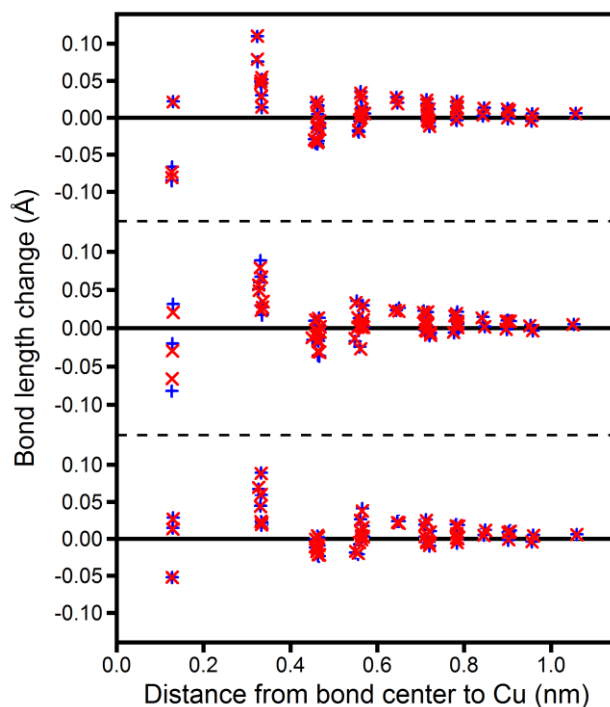**Figure S4.** Excited-state bond length changes for all Cu−Se and Cd−Se bonds in the Cu$^+$:Cd$_{33}$Se$_{34}$ NC, for the first three ^{1}ML$_{CB}$CT (blue + symbols) and first three ^{3}ML$_{CB}$CT (red ×symbols) excited states. Each singlet−triplet pair is shown on a different *y*-axis. These results are similar to those shown in Figure 5 of the main text for the Cu$^+$:Cd$_{76}$Se$_{77}$ NC, with the distortion centered around the Cu$^+$ dopant and the Cu−Se bond changes reflecting a totally symmetric contraction and asymmetric Jahn−Teller distortion.
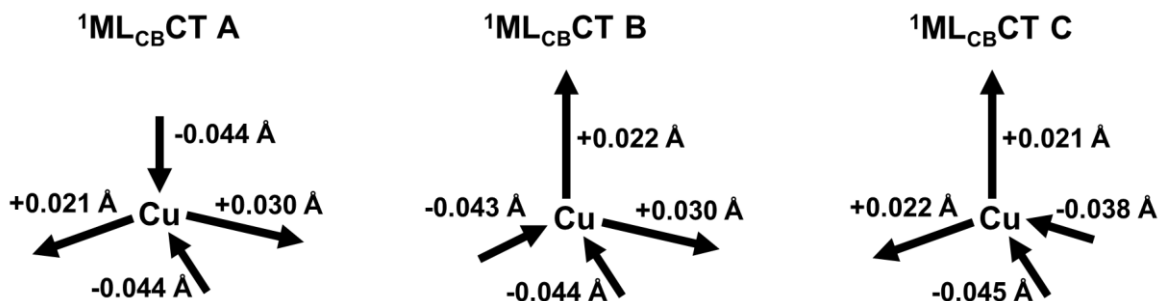

Figure S5. Calculated changes in Cu−Se bond lengths for the first three ^{1}ML$_{CB}$CT excited states of a Cu$^+$:Cd$_{76}$Se$_{77}$ NC. All three excited states involve a totally symmetric contraction and a Jahn−Teller distortion with T$_2$ symmetry, but each state has a different Jahn−Teller axis.

Table S4. Calculated ground-state geometry and complete list of excited-state distortions around Cu^+ (Cu−Se bond lengths, Se−Cu−Se bond angles, and dihedral angles) for the first six excited states of a Cu^+:$Cd_{33}Se_{34}$ NC with the Cu^+ located at the center of the NC.

	Ground state	$^1ML_{CB}CT$ A	$^3ML_{CB}CT$ A	$^1ML_{CB}CT$ B	$^3ML_{CB}CT$ B	$^1ML_{CB}CT$ C	$^3ML_{CB}CT$ C
r_{12} (Å)	2.579	-0.052	-0.051	-0.030	-0.020	0.021	0.022
r_{13} (Å)	2.579	-0.052	-0.051	-0.030	-0.020	0.021	0.022
r_{14} (Å)	2.580	0.014	0.015	-0.066	-0.082	-0.081	-0.085
r_{15} (Å)	2.579	0.027	0.029	0.021	0.032	-0.074	-0.066
θ_{213}	109.8	-5.5	-5.2	10.6	7.7	1.1	1.2
θ_{214}	109.3	2.0	2.1	-5.0	-4.5	1.9	1.5
θ_{215}	109.7	1.6	1.5	-2.0	1.0	1.6	2.0
θ_{314}	109.3	2.0	2.1	-5.0	-4.5	1.9	1.5
θ_{315}	109.7	1.6	1.5	-2.0	1.0	1.6	2.0
θ_{415}	109.1	-1.6	-1.9	3.5	-1.3	-8.6	-8.5
D_{5423}	70.6	1.7	1.7	0.0	-2.8	2.0	1.8
D_{5234}	70.4	-2.1	-2.1	1.7	6.3	-6.2	-6.3
D_{5342}	70.6	1.7	1.7	0.0	-2.8	2.0	1.8

Table S5. Calculated ground-state geometry and complete list of excited-state distortions around Cu^+ (Cu−Se bond lengths, Se−Cu−Se bond angles, and dihedral angles) for the first six excited states of a Cu^+:$Cd_{76}Se_{77}$ NC with the Cu^+ located at the center of the NC. The bond length changes for the $^1ML_{CB}CT$ excited states are illustrated in Figure S5.

	Ground state	$^1ML_{CB}CT$ A	$^3ML_{CB}CT$ A	$^1ML_{CB}CT$ B	$^3ML_{CB}CT$ B	$^1ML_{CB}CT$ C	$^3ML_{CB}CT$ C
r_{12} (Å)	2.576	-0.044	-0.018	0.022	0.020	0.021	0.021
r_{13} (Å)	2.576	0.021	-0.016	-0.043	-0.044	0.022	0.021
r_{14} (Å)	2.570	-0.044	-0.012	-0.044	0.000	-0.045	-0.042
r_{15} (Å)	2.569	0.030	-0.009	0.030	0.005	-0.038	-0.043
θ_{213}	109.3	2.9	6.4	2.5	-0.1	0.2	0.2
θ_{214}	109.4	-5.2	-2.8	0.9	1.4	0.9	1.7
θ_{215}	109.4	2.0	-2.8	-0.4	1.2	1.9	1.1
θ_{314}	109.4	0.5	-2.7	-5.2	-2.5	1.9	1.7
θ_{315}	109.4	-0.4	-2.7	2.2	-2.4	0.9	1.0
θ_{415}	109.8	0.2	5.0	0.0	2.2	-5.9	-5.8
D_{5423}	70.5	-1.2	-3.0	1.8	-1.5	0.9	1.2
D_{5234}	70.6	1.1	5.7	0.8	1.7	-4.5	-4.4
D_{5342}	70.5	1.5	-3.0	-1.2	0.4	1.9	1.3

Table S6. Calculated excited-state energies, measured relative to the ground state energy, before and after excited-state geometry relaxation, for the first six excited states of a Cu^+:$Cd_{33}Se_{34}$ NC with the Cu^+ located at the center of the NC. The nuclear reorganization energy is also shown. These energies are illustrated in Figure 3b of the main text.

	Energy with frozen geometry (eV)	Energy with relaxed geometry (eV)	Reorganization energy (eV)
$^1ML_{CB}CT$ A	2.699	2.463	0.236
$^1ML_{CB}CT$ B	2.728	2.426	0.302
$^1ML_{CB}CT$ C	2.748	2.409	0.339
$^3ML_{CB}CT$ A	2.649	2.427	0.222
$^3ML_{CB}CT$ B	2.675	2.389	0.286
$^3ML_{CB}CT$ C	2.703	2.386	0.317

Table S7. Calculated excited-state energies, measured relative to the ground state energy, before and after excited-state geometry relaxation, for the first six excited states of a Cu^+:$Cd_{76}Se_{77}$ NC with the Cu^+ located at the center of the NC. The nuclear reorganization energy is also shown. These energies are illustrated in Figure 3c of the main text.

	Energy with frozen geometry (eV)	Energy with relaxed geometry (eV)	Reorganization energy (eV)
$^1ML_{CB}CT$ A	2.414	2.221	0.193
$^1ML_{CB}CT$ B	2.416	2.227	0.189
$^1ML_{CB}CT$ C	2.423	2.216	0.207
$^3ML_{CB}CT$ A	2.380	2.188	0.192
$^3ML_{CB}CT$ B	2.381	2.205	0.176
$^3ML_{CB}CT$ C	2.391	2.200	0.191